

Perpendicular ultrasound velocity measurement by 2D cross correlation of RF data. Part A: validation in a straight tube

Bart Beulen · Nathalie Bijmens · Marcel Rutten ·
Peter Brands · Frans van de Vosse

Received: 1 August 2009 / Revised: 2 March 2010 / Accepted: 15 March 2010 / Published online: 2 April 2010
© The Author(s) 2010. This article is published with open access at Springerlink.com

Abstract An ultrasound velocity assessment technique was validated, which allows the estimation of velocity components perpendicular to the ultrasound beam, using a commercially available ultrasound scanner equipped with a linear array probe. This enables the simultaneous measurement of axial blood velocity and vessel wall position, rendering a viable and accurate flow assessment. The validation was performed by comparing axial velocity profiles as measured in an experimental setup to analytical and computational fluid dynamics calculations. Physiologically relevant pulsating flows were considered, employing a blood analog fluid, which mimics both the acoustic and rheological properties of blood. In the core region ($|r/a| < 0.9$), an accuracy of 3 cm s^{-1} was reached. For an accurate estimation of flow, no averaging in time was required, making a beat to beat analysis of pulsating flows possible.

1 Introduction

In clinical practice, ultrasound is often used as a non-invasive method to assess blood velocity and vessel wall motion (Brands et al. 1999). These parameters are related to local blood volume flow and local pressure, respectively, which play a major role in cardiovascular (dys)function.

Simultaneous assessment of pressure and flow facilitates accurate vascular impedance estimation, which is a valuable tool in determining the condition of the vascular tree.

Doppler ultrasound allows an accurate assessment of the component of the blood velocity along the ultrasound beam. To assess the axial blood velocity component, the ultrasound beam has to be positioned at an angle with respect to the blood vessel. For a reliable velocity assessment, it is necessary that this angle is accurately known, since small deviations already result in large velocity errors (Fillinger and Schwartz 1993; Gill 1985). To relate the velocity measurement to volume flow, assumptions have to be made on the axial velocity distribution across the vessel. The position of the vessel walls needs to be accurately known in order to perform the integration from velocity to flow. Furthermore, an accurate assessment of vessel wall motion is required for local pressure estimation from the flow/area relation (Rabben et al. 2004). However, the position of the vessel walls can only be assessed accurately with the ultrasound beam in perpendicular orientation with respect to the vessel. This renders a simultaneous measurement of velocity by Doppler ultrasound and wall position impossible, hampering an accurate flow assessment. Furthermore, most arteries are tapered, curved and bifurcating, causing the axial velocity distribution to be altered by transversal velocities, resulting in asymmetrical axial velocity profiles and consequently in inaccurate flow estimations (Krams et al. 2005). For volume flow estimation in curved vessels, the reader is referred to part B of this article (Beulen et al. 2010).

Several blood velocity measurement techniques based on ultrasound have been reported to overcome the angle dependency of Doppler ultrasound and to allow 2D velocity estimation. Vector Doppler methods were introduced, in which ultrasound beams, angled with respect to

B. Beulen · N. Bijmens (✉) · M. Rutten · F. van de Vosse
Section Cardiovascular Biomechanics,
Department of Biomedical Engineering,
Eindhoven University of Technology,
PO Box 513, 5600 MB Eindhoven, The Netherlands
e-mail: n.bijmens@tue.nl

P. Brands
ESAOTE Europe, PO Box 1132,
6201 BC Maastricht, The Netherlands

each other, were applied to assess the 2D velocity, using either a single transducer (Fox 1978) or two (Overbeck et al. 1992). The drawback of these methods is that for increasing distance, deviation and bias in the velocity estimate increases.

Ultrasound speckle velocimetry (USV) allows flow imaging with a high spatial resolution and a negligible angle dependency (Bohs et al. 1993, 1995; Sandrin et al. 2001; Trahey et al. 1987). The USV technique enables assessment of 2D velocity vectors by analyzing the acoustic speckle pattern of the flow field. However, for an accurate, low noise velocity assessment, this technique requires specially modified ultrasound systems, custom scanning sequences and custom-developed ultrasound transducers (Bohs et al. 2000; Sandrin et al. 2001). To induce a large amount of scattering, high concentrations of scattering particles are applied. However, due to the requirement of very high particle concentrations (Kim et al. 2004a), the application of USV for in vivo applications is limited. Additionally, the presence of velocity gradients seriously affects the USV performance (Adrian 1991).

Jensen and Munk (1998) introduced the transverse oscillation (TO) method, which is based on the principle of applying a transverse spatial modulation to enable the assessment of motion transverse to the ultrasound beam. Both experiments in an experimental setup and in vivo (Udesen and Jensen 2003, 2004) have shown that the TO method allows an accurate assessment of blood velocity for transverse flow. Although at this point, experimental ultrasound systems are used to implement the TO method, this method may have the potential of being implemented in a commercial scanner for real-time estimation.

The application of particle image velocimetry (PIV) techniques (Adrian 2005) to ultrasound was first reported by Crapper et al. (2000). PIV algorithms were applied to B-mode video images of a sediment-laden flow, resulting in estimated velocities up to 6 cm s^{-1} . Kim et al. (2004a, b) introduced Echo PIV: advanced PIV algorithms were applied on second harmonic images enhanced by an ultrasound contrast agent (UCA), generated by a commercially available ultrasound scanner equipped with a phased array sensor transducer. This allowed the assessment of the 2D velocity field, with a spatial resolution of $1.2 \times 1.7 \text{ mm}$ at the image center. For steady flow, a dynamic range of $1\text{--}60 \text{ cm s}^{-1}$ was reported, obtained at a temporal resolution of 3.8 ms. For pulsating flow, 18 cycles were ensemble averaged to obtain axial velocity profiles with a peak velocity up to 50 cm s^{-1} at a temporal resolution of 2 ms. Liu et al. (2008) developed a custom-designed ultrasound system equipped with a linear array probe to ensure a more uniform axial and lateral resolution compared to the phased array transducer. The custom-designed system allowed

flexible control of the Echo PIV parameters. A comparison between Doppler and echo PIV-based measured peak velocity on high speed non-laminar flow up to 140 cm s^{-1} showed a maximum deviation of 6.6%. For the measured flow rates, echo PIV imaging parameters such as frame rate, beam line density and spatial resolution were adjusted such that the maximum velocity was accurately captured.

In this study, an ultrasound velocity assessment technique similar to echo PIV, which focusses on the assessment of the velocity component perpendicular to the ultrasound beam, is applied. This makes a simultaneous assessment of axial velocity profile and vessel wall position possible, thereby enabling an accurate assessment of volume flow and facilitating a simultaneous pressure estimation. Contrary to the previously summarized velocity assessment techniques, the validation is performed in an experimental setup, in which physiological flows are generated using a fluid, which mimics both the acoustic and rheological properties of blood. Velocity profile measurements are performed by applying PIV-based analysis techniques to raw RF-data acquired with a commercially available, clinically approved ultrasound system, equipped with a linear array transducer. Resulting velocity profiles are compared to analytical and computational fluid dynamics (CFD) calculations. Finally, the velocity profiles are integrated to volume flow and compared to reference flow measurements.

2 Materials and methods

2.1 Experimental setup

In the experimental setup (Fig. 1), a fluid, mimicking the acoustic and rheological properties of blood, is pumped from a reservoir through a compliant tube, which mimics the blood vessel. A polyurethane tube (HemoLab, Eindhoven, The Netherlands) with a length of about 1.5 m, a radius of 4 mm and a wall thickness of 0.1 mm is applied to mimic the common carotid artery (CCA). The tube is fully submerged in a reservoir of water to prevent deformation under influence of gravity. Additionally, the water acts as an excellent conductor of sound. The tube is terminated by an impedance from which the fluid flows back, through a reservoir, to the inlet of the pump. For the terminal impedance, a Windkessel model is applied. The viscous dissipation in the distal vessel, R , and the viscous dissipation in the distal capillary bed R_p , are modeled by local narrowing, the compliance of the arterial system, C , is modeled by an air-chamber.

The flow is generated by combining a steady pump and a servo-actuator operated piston pump (indicated in Fig. 1 by a single symbol). The steady pump (Pacific Scientific, IL,

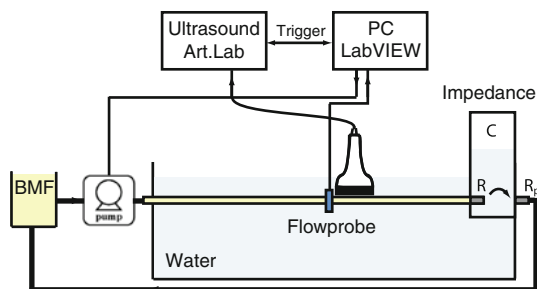


Fig. 1 Schematic overview of the experimental setup

USA) is manually set to a specific flow rate, whereas the trajectory of the piston pump (home developed) is computer controlled with LabVIEW software (National Instruments, Austin, TX, USA).

The ultrasound probe is placed far (approximately 1 m) from the inlet of the polyurethane tube to ensure development of laminar flow at the measurement site. By means of a 3D manipulator, the probe is accurately positioned perpendicularly to the vessel by looking for the highest intensity. Hence, the mechanical focus of the probe is located at the centerline of the vessel. To maximize the signal level, the electrical focus is set equal to the mechanical focus. At about 1 cm upstream of the ultrasonic probe, a flow probe with an accuracy of 5% (Transonic, 10PAA) is positioned to measure the flow through the vessel. The data from the flow probe measurements are acquired simultaneously with the data from the ultrasound scanner, using a common trigger signal generated by a PC using the same LabVIEW software.

2.2 Blood mimicking fluid

Blood is a non-Newtonian fluid with shear thinning properties: for high shear rates, the viscosity decreases. A shear thinning blood mimicking fluid (BMF), with both acoustical and mechanical properties similar to blood has been developed.

The BMF consists of Xanthan gum (Fluka, 95465), 0.5 g l^{-1} dissolved in water (97.3% weight) with 1.8% weight Orgasol particles and 0.9% weight Synperonic NP10 added. Xanthan gum is used to mimic the mechanical behavior of blood (Brookshier and Tarbell 1993; van den Broek et al. 2008). Ultrafine polyamide particles (2001UDNAT1, Orgasol, ELF Atochem, Paris, France) with a diameter of $5 \times 10^{-6} \text{ m}$ are used as ultrasound scattering particles. The polyamide particles have a specific density of 1.03 g cm^{-3} . It is known that for a BMF consisting of particles with a size of $5 \times 10^{-6} \text{ m}$, a concentration of 1.8% by weight is needed in order to obtain a blood-similar backscattering of ultrasound waves (Ramnarine et al. 1998). Synperonic NP10 (Fluka 86208) acts as a surfactant to prevent coagulation of the Orgasol particles.

In general, scattering particles used in BMF are chosen to be naturally buoyant (Ramnarine et al. 1998) with respect to the fluid base. This implies an accurate control of the fluid density to prevent the particles to sediment or float. The shear thinning properties of the developed BMF reduce sedimentation and floating of particles since slow moving particles experience a relatively high drag force, due to high viscosity at low shear. This facilitates the application of the BMF in the phantom setup.

The velocity distribution across the vessel cannot be described by Poiseuille (steady flow) or Womersley (unsteady flow) theory, since these were derived for Newtonian fluids. Mathematically, the BMF can be modelled as a generalized, non-Newtonian shear thinning liquid. Application of a power-law model (Bird 1987) enables an analytic approach for calculating the velocity distribution. The power-law model is given by

$$\eta = \eta_0 (\lambda \dot{\gamma})^{n-1}, \quad (1)$$

with η_0 the viscosity at $\dot{\gamma} = 1/\lambda$, a time constant λ and n the power-law constant. The power-law model can only be applied to describe the viscosity at intermediate shear rates, since very low and very high shear rates result in physically unrealistic values for the viscosity.

Assuming that the non-Newtonian properties of a fully developed, steady flow can be characterized by a power-law model at characteristic shear rate, the velocity distribution for fully developed flow in a straight circular tube is given by Bird (1987):

$$v(r) = \frac{Q}{\pi a^2} \frac{1}{\frac{1}{2} - \frac{1}{n+3}} \left(1 - \left(\frac{r}{a} \right)^{\frac{n+1}{n}} \right), \quad (2)$$

in which $n = n(\dot{\gamma}_{\text{char}})$. The characteristic shear rate $\dot{\gamma}_{\text{char}}$ is defined as (Gijzen et al. 1999):

$$\dot{\gamma}_{\text{char}} = \frac{2Q}{\pi a^3}, \quad (3)$$

in which Q is volume flow rate through the vessel and a , the radius of the vessel. Consequently, for shear thinning fluids, this results in velocity profiles that are flattened ($n < 1$) compared to the Poiseuille profiles for Newtonian flow ($n = 1$).

A more realistic viscosity model, which can be applied in CFD analysis, is given by the Carreau-Yasuda model (Bird 1987):

$$\frac{\eta - \eta_\infty}{\eta_0 - \eta_\infty} = [1 + (\lambda \dot{\gamma})^b]^{(n-1)/b}, \quad (4)$$

with η_0 the viscosity at low shear rate, η_∞ the viscosity at high shear rate, λ a time constant and n the power-law constant. The parameter b determines the transition between the low-shear-rate region and the power-law region.

2.3 Data acquisition

In ultrasound imaging, an ultrasonic pulse is transmitted into a test medium. Subsequently, the echo (RF) signal, consisting of contributions due to scattering and reflections, is received. By time of flight analysis, the depth information corresponding to the RF-signal is obtained. Analysis of the scattering and reflection contributions in the RF-signal allows to estimate tissue and blood flow properties.

In this study, the commercially available Picus Art.Lab ultrasound system (ESAOTE Europe, Maastricht, The Netherlands) is used to collect the raw RF-data for offline processing. The system is equipped with a 7.5 MHz linear array transducer of 40 mm, consisting of 128 transducer elements. The RF-data are sampled at 33 MHz (f_s) and have an approximate center frequency of 6.8 MHz and a quality factor (the center frequency divided by the bandwidth) of 2.

For the PIV measurements, the ultrasound system is operated in fast B-mode (high frame rate B-mode), also called multiple M-line mode. Each frame is composed of 14 adjacent M-mode lines generated at a pitch of 0.315 mm. To maximize the signal level at the focal point, the electrical focus is set equal to the mechanical focus, which is fixed at 2 cm from the transducer surface. The frame rate of the ultrasound system is determined by the number of M-lines and the pulse repetition frequency (f_{pr}), the frequency at which individual M-mode lines are acquired, which depends on the maximum depth setting of the ultrasound system. For the PIV measurements the depth is set to 50 mm, which results in a frame rate, f , of 730 s^{-1} . The maximum measurement time is hardware limited to about 3.8 s. The RF-data matrix obtained from the system is a 3D function of depth (r), time (t) and position along the probe (z) (Fig. 3).

2.4 Data processing

The RF-data were processed on a PC using Matlab (The MathWorks, Natick, MA, USA). After removal of the DC component of the RF signals, a 4th order Butterworth band pass filter (4.2 and 12.5 MHz) according to the quality factor of the ultrasound beam is applied. A 4th order Butterworth high pass filter with a cutoff frequency of 20 Hz is applied in the temporal direction to suppress static and slow moving objects (e.g. wall reverberations).

A cross-correlation-based technique similar as in PIV (Adrian 2005) is applied to determine the axial velocity distribution of the flow through the tube. In optical PIV, the spatial resolution is determined by the number of pixels in the image sensor in combination with the interrogation area size. In the case of a square data area, this results in an equal resolution for both spatial directions. For the

ultrasound data, the field of view (FOV) is rectangularly shaped (Fig. 2). The width of the FOV is determined by the transducer element width, W_{el} , which is equal to $0.315 \times 10^{-3} \text{ m}$, and the number of active transducer elements. For 14 adjacent M-mode lines and an imaging depth set to 50 mm this results in a FOV of $4.4 \times 50.0 \text{ mm}$.

The spatial resolution along the ultrasound beam, determined by the ultrasound wavelength, is much higher than the resolution in perpendicular direction, which depends on the overall size of the aperture, the degree of focusing, the ultrasound frequency and the imaging depth. Because of this, data windows applied to the RF-data have a small width of 0.2 mm in radial direction and are rather large width of 4.4 mm (14 M-mode lines) in axial direction. Taking into account, the sample rate of 33 MHz and the velocity of the ultrasound wave in water ($1,510 \text{ m s}^{-1}$), 0.2 mm in radial direction corresponds to eight samples. The axially stretched data windows are consistent with the objective to accurately assess axial velocity profile and flow through vessels: the small radial dimension of the data window allows the estimation of axial velocity in the presence of large radial gradients, additionally, the axial gradients in axial velocity are presumed to be small compared to the radial gradients, justifying the large axial dimension of the data window.

The anterior (ξ_a) and posterior wall positions (ξ_p) have been identified by means of a sustain attack filter (Meinders et al. 2001). The sustain attack filter is an automatic edge detector based on constructing a reference signal, decaying as a function of depth. The filter works on the envelope of the RF-data. For the cross-correlation, 50% overlapping data windows are applied to the lumen of the vessel. Positions along the coordinate axis ξ are expressed in ultrasound sample points. The data windows are indicated by their respective center coordinate ξ_w^i , in which $1 \leq i \leq N$, with N the total number of applied data windows in a single frame. The position of the data windows, expressed in meters, r_w^i , with respect to the centerline is given by

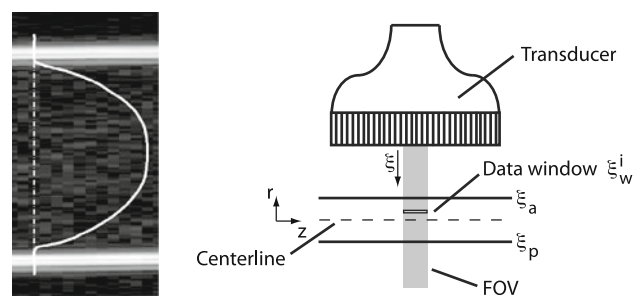


Fig. 2 B-mode image of the RF-data with a typical velocity profile (left) and a schematic overview of the field of view (right). The anterior (ξ_a) and posterior wall position (ξ_p) of the vessel is indicated as well as a rectangular data window ξ_w^i used for cross-correlation. It should be noted that individual particles are not visible

$$r_w^i = \frac{2c}{f_s} \left[\zeta_w^i - \frac{\zeta_p + \zeta_a}{2} \right], \tag{5}$$

in which c is the velocity of sound for the BMF and f_s the ultrasound sampling frequency. The vessel radius is determined by

$$a = \frac{c}{f_s} (\zeta_p - \zeta_a). \tag{6}$$

Like in optical PIV analysis, for each data window in the acquired frames, the shift between two corresponding data windows from subsequent frames was calculated by performing a 2D cross-correlation in the time domain on the raw RF-data and determination of the peak position in the cross-correlation plane (Fig. 3).

The position of the peak, $\delta \hat{\mathbf{x}}(r_w^i) = (\delta \hat{\zeta}(r_w^i), \delta \hat{z}(r_w^i))$, is determined by finding the location of the maximum in the correlation plane after application of a Hilbert transformation, which is applied to calculate the envelope. According to the central limit theory (Evans et al. 2000), the backscattered echo is Gaussian distributed since it is composed of signal contributions due to many independent scatters (Cloutier et al. 2004). Consequently, to gather sub-pixel information for the peak position, a three point Gaussian-fit estimator (Westerweel 1993) is applied for

determining the fractional displacement $\epsilon(r_w^i) = (\epsilon_\zeta(r_w^i), \epsilon_z(r_w^i))$.

$$\epsilon_\psi(r_w^i) = \frac{\ln(\delta \hat{\psi}(r_w^i) - 1) - \ln(\delta \hat{\psi}(r_w^i) + 1)}{2[\ln(\delta \hat{\psi}(r_w^i) - 1) + \ln(\delta \hat{\psi}(r_w^i) + 1) - 2\ln(\delta \hat{\psi}(r_w^i))]} \tag{7}$$

for $\psi = \zeta, z$.

For each data window, this resulted in the sub-pixel peak position, with respect to the center of the cross-correlation plane, $\delta \hat{\mathbf{x}}(r_w^i) = \delta \hat{\mathbf{x}}(r_w^i) + \epsilon(r_w^i)$. The position of the peak with respect to the center of the cross-correlation plane, $\delta \hat{\mathbf{x}}(r_w^i)$, provides an estimate of both the average radial and average axial velocity of the fluid inside the data window. Regarding the fact that a single frame is composed from multiple M-mode lines acquired at the f_{pr} (ultrasound B-mode imaging is a swept process), the axial velocity was calculated from the axial shift, $\delta z(r_w^i)$, by

$$v_z(r_w^i) = \frac{\Delta z}{\Delta t} = \frac{W_{el} \delta z(r_w^i)}{f^{-1} + f_{pr}^{-1} \delta z(r_w^i)}, \tag{8}$$

in which Δz is the axial shift expressed in meters and Δt the actual time difference in seconds corresponding to the axial shift. It should be remarked that $f_{pr}^{-1} \delta z(r_w^i)$ corrects for the time needed to sweep to the M-mode line corresponding to the axial shift $\delta z(r_w^i)$. The + sign indicates that the sweeping direction of the scanner and the direction of the flow are the same. The radial velocity can be calculated from the radial shift, $\delta \zeta(r_w^i)$, by

$$v_r(r_w^i) = \frac{\Delta r}{\Delta t} = \frac{2c \delta \zeta(r_w^i)}{f_s f^{-1}}, \tag{9}$$

in which Δr is the radial shift expressed in meters and Δt the actual time difference in seconds corresponding to the radial shift. In this study, only the axial velocity was assessed, since no radial velocity components are present for developed flow in a straight vessel.

2.5 Validation

The cross-correlation-based velocity estimation method was applied to measure axial velocity profiles for both fully developed steady and unsteady flows. The assessed profiles were compared to analytical solutions and CFD computations for the axial velocity profile based on the blood volume flow as estimated by means of the flow probe. The kinematic viscosity of the BMF was measured as function of shear rate with a Couette rheometer (RFS 2, Rheometrics Scientific) in order to calculate axial velocity profiles. A least squares fit of Eq. (4) was performed to estimate the parameters in the Carreau-Yasuda model.

The steady flow was generated with a constant head system positioned between the steady pump and the inlet of the phantom vessel to attenuate possible flow oscillations

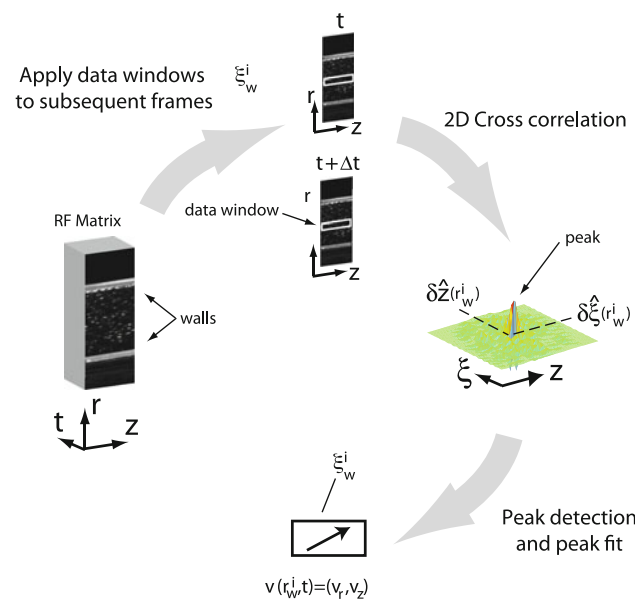


Fig. 3 Schematic overview of the velocity estimation algorithm. For all frames in the RF matrix, data windows, ζ_w^i , are applied. For each pair of corresponding data window in subsequent frames a cross-correlation is performed. The shift between the data windows is estimated by detecting the peak position, $\delta \hat{\mathbf{x}}(r_w^i) = (\delta \hat{\zeta}(r_w^i), \delta \hat{z}(r_w^i))$, in the cross-correlation plane and subsequently performing a peak fit. By incorporating the time difference between subsequent frames, the average velocity, $\mathbf{v}(r_w^i, t)$, of the fluid corresponding to the data window is determined from the estimated shift

caused by the steady pump. By varying the resistance, R , at the outlet of the phantom vessel, steady flow rates ranging from 0.23 to 1.23 l min⁻¹ were generated, corresponding to characteristic shear rates (3) of 38 and 204 s⁻¹, respectively. Using these values, the Reynolds number, Re defined as:

$$Re = \frac{2a\bar{v}\rho}{\eta(\dot{\gamma}_{\text{char}})}, \quad (10)$$

in which \bar{v} is the average axial velocity and ρ the BMF density, ranges from 75 to 800. The Womersley number, α is defined by:

$$\alpha = a\sqrt{\frac{\omega\rho}{\eta}}, \quad (11)$$

and ranges from 8 to 12.

Flow rates were measured by means of the flow probe, which was calibrated before each measurement using a stopwatch and a measuring beaker. For each flow rate an ultrasound measurement was performed. The RF-data were filtered as described in the previous section. Application of the cross-correlation algorithm resulted in a 2,816 instantaneous velocity profile estimations, sampled at 730 Hz. A median filter with a temporal and spatial window size of, respectively, 4×10^{-3} s and 6.9×10^{-5} m, was applied to remove outliers. The average velocity profile measurement was compared with the analytic approximation of the velocity profile as defined in (2). The power-law constant, n , was assessed by determining the tangent to the Carreau-Yasuda curve at the characteristic shear rate. The characteristic shear rate was based on the mean flow estimate of the flow probe.

For the unsteady flow measurements, a pulsatile flow waveform with a cycle time of 1 s, a mean of about 0.7 l min⁻¹ and a peak flow of about 1.5 l min⁻¹ was generated by superimposing the flow pulse of the piston pump on the steady flow of the steady pump. This corresponds to an average Reynolds number of 300 and a peak Reynolds number of 900 which is physiologically relevant (Ku et al. 1985). The impedance at the outlet was set such that the induced pressure was high enough to prevent the vessel to collapse but small enough to lead to a negligibly small vessel wall motion. Using LabVIEW, the piston pump was programmed to generate 30 beats. Simultaneously, the flow was measured. During these 30, 3.8 s of fast B-mode RF-data were obtained for offline processing. The trigger signal was used to synchronize the flow measurement with the RF-data. The RF-data were filtered as described in the previous section. Application of the cross-correlation algorithm resulted in 2,816 instantaneous velocity profile estimations, sampled at 730 Hz. After the removal of outliers by application of a median filter with a temporal and spatial window size of respectively,

4×10^{-3} s and 6.9×10^{-5} m, a low pass, zero-phase Butterworth filter with a cut-off frequency of 40 Hz was applied to suppress high frequency noise. So no beat-to-beat averaging was performed allowing for real-time flow assessment in future ultrasound systems.

A finite-element CFD model of a rigid walled straight tube (Beulen et al. 2009; van de Vosse et al. 2003) was applied to calculate the time-dependent velocity distribution across the vessel. The shear rate dependency of the viscosity was incorporated by implementing the Carreau-Yasuda model (4) in the CFD model. For the boundary conditions, at the inlet, the flow as assessed in the experiments was prescribed, at the walls, the no-slip condition was applied. The results of the instantaneous velocity profile measurement were compared with the CFD computations.

Subsequently, the flow measurements were compared to flow estimates based on the integration of the measured axial velocity profiles.

3 Results

3.1 Blood mimicking fluid

The viscosity was determined for shear rates between 0.1 s⁻¹ and 1,000 s⁻¹ with ten measurements per decade (Fig. 4).

The parameters η_0 , η_∞ , λ , a and n , of the Carreau-Yasuda model describing the BMF were determined with a least squares fit of (4) on the viscosity data presented in Fig. 4 and are presented in Table 1. The calculated correlation coefficient between the measured values and the fitted values was 0.9987.

The speed of sound was assessed by a time of flight measurement using a single ultrasound transducer in a well-known geometry. From the measurement of time differences δt and the known distances δx a speed of sound equal to 1,510 m s⁻¹ was calculated at room temperature.

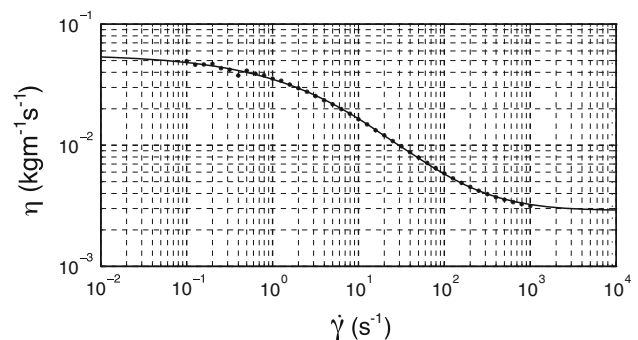


Fig. 4 Shear thinning behavior of the BMF, *filled circle* indicates measurements, the *solid line* indicates the fit

Table 1 Parameters of the Carreau-Yasuda model describing the BMF as estimated by means of a least squares linear fit

η_0 ($\text{kgm}^{-1}\text{s}^{-1}$)	η_∞ ($\text{kgm}^{-1}\text{s}^{-1}$)	λ (s)	b	n
5.6×10^{-2}	2.9×10^{-2}	1.0×10^{-1}	5.3×10^{-1}	-4.6×10^{-2}

The density of the BMF was calculated by measuring the mass of a known volume of BMF (volumetric pipette) by means of a Mettler balance and was found to be equal to $1,100 \text{ kg m}^{-3}$.

3.2 Steady flow

For each measurement, the flow rate, the Reynolds number, the corresponding characteristic shear rate and the resulting power-law constant are presented in Table 2. A comparison between the mean velocity profiles for the ultrasound measurement and the analytic solution of the velocity profile is shown in Fig. 5. The results were non-dimensionalized by the radius a , of the vessel. The ultrasound transducer was located at $r/a \approx -5$.

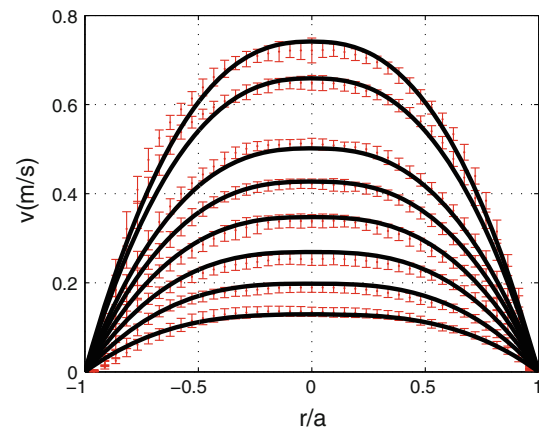
Excellent agreement was found between the analytic solution and the ultrasound measurements. The root mean square value of the deviation between the measured and calculated velocity profiles ranges from 1 cm s^{-1} , for the lowest flow rate, to 4 cm s^{-1} , for the higher flow rates. For the two highest flow rates (1.10 and 1.23 l min^{-1}), the measured flow profiles appear to be more flat than the calculated velocity profiles.

3.3 Unsteady flow

A comparison between the instantaneous velocity profile measurement and the CFD solution of the velocity profile is presented in Fig. 6. The velocity profiles are shown at 8 distinct phases in the period. The results were non-dimensionalized by the radius, a , of the vessel. Again the ultrasound transducer was located at $r/a \approx -5$.

Table 2 Overview of the flow rate, Reynolds number and the characteristic shear rate

Q (l min^{-1})	Re	$\dot{\gamma}_{\text{char}}$ (s^{-1})
0.23	75	38
0.35	140	58
0.47	214	78
0.60	302	100
0.73	397	120
0.85	489	141
1.10	691	182
1.23	800	204

**Fig. 5** Comparison of the ultrasound measurement and the analytic velocity profile (filled circle ultrasound measurement; solid line analytic solution)

Overall, the measurements agree very well with the calculated velocity profiles, although minor deviations occur in the near wall region. Especially, during the systolic peak deviations between calculation and measurement occur. Near $r/a = -0.5$, significant fluctuations of the assessed velocity occur due to an ill-suppressed reverberation.

Integration of the velocity profile over the cross sectional area of the vessel results in a flow estimate. A comparison of the ultrasound-based flow estimate and the direct volume flow measurement is presented in Fig. 7. To both flow waveforms a low pass, zero-phase Butterworth filter with a cut-off frequency of 40 Hz was applied to suppress high frequency noise.

Both flow waveforms agree very well, no significant deviations occurred.

4 Discussion

The steady flow measurements indicate that the deviation between the time averaged ultrasound velocity measurement and the analytic solution in the core region is at most about 3 cm s^{-1} . For the highest flow rate, the measured velocity profile appears to be more flat than the calculated velocity profile. Here, the velocity limit of the PIV correlation method is reached, resulting in false-positive correlations giving rise to lower velocities in the middle of the vessel. For the measurements at lower flow rates, there is a good agreement between the measured values and the CFD values. For both the steady and unsteady flow, the deviation between calculated and measured velocity profile increases in the near wall region, $0.9 < |r/a| < 1.0$. This can be caused by the fact that the signal of the wall dominates the scattering signal in this region, which results in errors in the velocity estimation.

Fig. 6 Comparison of the ultrasound measurement and the calculated velocity profile (*open circle* ultrasound measurement; *solid line* CFD calculation)

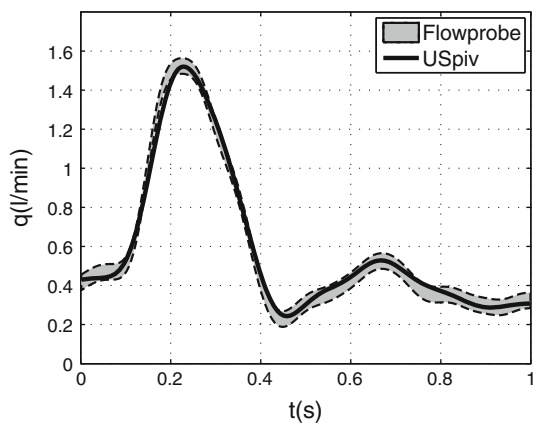
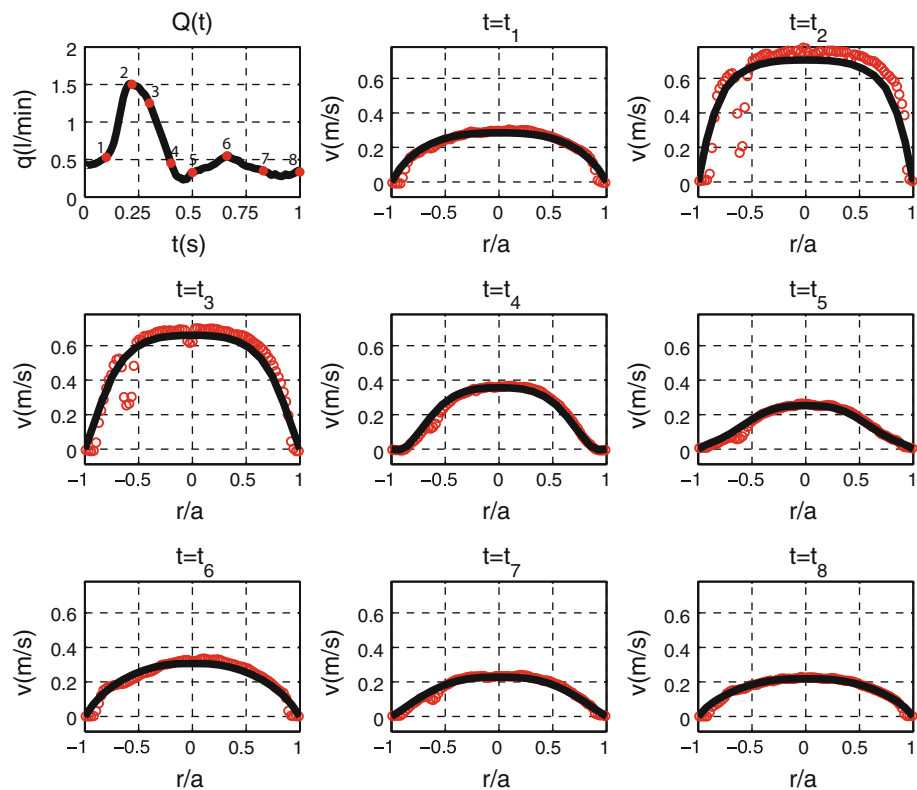


Fig. 7 Comparison of the ultrasound-based flow estimate and the flow probe estimate

For the unsteady flow, at peak systole, a drop of signal occurs at $r/a \approx -0.7$, which is approximately the position at which the reverberation of the anterior wall appears. For steady flow, the reverberation is static, allowing the high pass filter to suppress the reverberation. However, for unsteady flow, the reverberation is slightly moving. As a result, the applied high pass filter is not able to adequately suppress the reverberations. Furthermore, the velocity approximation is found to be systematically high from $r = -0.5$ to $r = 0.9$ for t_2 and t_3 . The small deviations observed are probably caused by measurement errors

caused by the flow probe, which result in errors in the CFD-derived velocity profiles.

Kim et al. (2004b) have shown that the accuracy and resolution of EchoPIV are improved by application of iterative schemes (Hart 2000) and smart window offsetting (Westerweel et al. 1997). In principle, these techniques could be applied to the RF-data acquired in this study. Although the resolution in radial direction is sufficient, in axial direction, some improvement is desired. However, in axial direction only 14 samples are available, limiting the application of the earlier mentioned techniques.

Before a practical in vivo application of the velocity estimation technique is possible, a few issues need to be considered.

First, the ultrasonic backscatter from flowing blood is found to be dependent on the local hemodynamics (Yuan and Shung 1989). The resulting variation in echogenicity is probably caused by the combined effect of shear rate and acceleration on red blood cell aggregation (Paeng et al. 2004a, b). A drop in echogenicity could have an adverse effect on the accuracy of velocity estimation. To study these consequences, actual blood should be applied in the phantom setup, since for the BMF no aggregation of the scatterers occurs, resulting in a constant echogenicity.

Secondly, in vivo most arteries are curved, resulting in secondary velocity components and an asymmetric axial velocity distribution. The secondary velocity components

will result in a motion of the scatterers, transverse to the measurement plane. This may have an adverse effect on the accuracy of velocity estimation. Furthermore, measurements of the axial velocity distribution will result in asymmetric velocity profiles, for which the integration to obtain flow is not trivial. Both consequences will be looked into in upcoming studies.

Finally, probably the biggest challenge for implementation of the velocity estimation technique for in vivo application is the development of proper clutter removal filters. As in vivo, the relative strength of the wall signal with respect to the blood signal is about 60 dB higher, signifying the importance of these filters. The unsteady flow measurements have shown that reverberations can cause significant errors in the velocity estimation and that adequate filtering is required to suppress these wall signals. In the phantom setup, the reverberation occurs at a discrete position because of the uniform vessel wall thickness and properties. As a result, the velocity estimation is disrupted only locally. However, in vivo, reverberations are present throughout the lumen, further complicating the velocity estimation.

Under the assumption that an adequate anti-clutter filter can be developed, this technique allows a beat to beat analysis of the velocity distribution/flow using a commercially available and clinically approved ultrasound system. In the future, a real-time assessment might be possible, since no averaging is required. Furthermore, in combination with pulse wave velocity and distension measurements, a simultaneous assessment of pressure and flow will be enabled. This will allow ultrasound to be extended from a local property to a global properties assessment method in clinical practice.

5 Conclusion

An ultrasound velocity assessment technique is introduced, which allows the estimation of velocity components perpendicularly to the ultrasound beam, using a commercially available ultrasound scanner equipped with a linear array probe. Validation measurements in a phantom setup, with the linear array probe in perpendicular orientation with respect to the vessel have shown that a beat to beat assessment of the axial velocity profile is feasible. In the core region ($|r|/a < 0.9$), an accuracy of 3 cm s^{-1} is achieved; in the near wall region ($0.9 < |r|/a < 1$), the accuracy decreases due to the presence of the wall. For a physiologically relevant flow, a successful integration from velocity profile to flow has been performed indicating that this technique can be a valuable asset for an accurate flow estimation in vessels in clinical applications.

Acknowledgments This work is part of and was supported by EUREKA project E!3399 ART.MED, IS042015.

Open Access This article is distributed under the terms of the Creative Commons Attribution Noncommercial License which permits any noncommercial use, distribution, and reproduction in any medium, provided the original author(s) and source are credited.

References

- Adrian RJ (1991) Particle-imaging techniques for experimental fluid mechanics. *Annu Rev Fluid Mech* 23:261–304
- Adrian RJ (2005) Twenty years of particle image velocimetry. *Exp Fluids* 39:159–169
- Beulen BWAMM, Rutten MCM, van de Vosse FN (2009) Fluid structure interaction in distensible vessels: a time periodic coupling. *J Fluids Struct* doi:10.1016/j.jfluidstructs.2009.03.002
- Beulen BWAMM, Verkaik AC, Bijmens N, Rutten MCM, van de Vosse FN (2010) Perpendicular ultrasound velocity measurement by 2d cross correlation of RF data. Part B: volume flow estimation in curved vessels. *Exp Fluids*. doi:10.1007/s00348-010-0866-4
- Bird RB (1987) Dynamics of polymeric liquids, vol 2. Wiley, New York
- Bohs LN, Friemel BH, McDermott BA, Trahey GE (1993) A real time system for quantifying and displaying two-dimensional velocities using ultrasound. *Ultrasound Med Biol* 19(9):751–761
- Bohs LN, Friemel BH, Trahey GE (1995) Experimental velocity profiles and volumetric flow via two-dimensional speckle tracking. *Ultrasound Med Biol* 21(7):885–898
- Bohs LN, Geiman BJ, Anderson ME, Gebbart SC, Trahey GE (2000) Speckle tracking for multi-dimensional flow estimation. *Ultrasonics* 38:369–375
- Brands PJ, Hoeks APG, Willigers JM, Willekes C, Reneman RS (1999) An integrated system for the non-invasive assessment of vessel wall and hemodynamic properties of large arteries by means of ultrasound. *Eur J Ultrasound* 9:257–266
- Brookshier KA, Tarbell JM (1993) Evaluation of transparent blood analog fluid: aqueous xanthan gum/glycerin. *Biorheology* 30:107–116
- Cloutier G, Daronat M, Savery D, Garcia D, Durand LG, Foster SF (2004) Non-Gaussian statistics and temporal variations of the ultrasound signal backscattered by blood at frequencies between 10 and 58 MHz. *J Acoust Soc Am* 116(1):566–577
- Crappier M, Bruce T, Gouble C (2000) Flow field visualization of sediment-laden flow using ultrasonic imaging. *Dyn Atmos Oceans* 31:233–245
- Evans M, Hastings N, Peacock B (2000) Statistical distributions. Wiley, New York
- Fillinger MF, Schwartz RA (1993) Volumetric blood flow measurements with color Doppler ultrasonography: the importance of visual clues. *J Ultrasound Med* 3:123–130
- Fox MD (1978) Multiple crossed-beam ultrasound Doppler velocimetry. *IEEE Trans Son Ultrason* SU 25:281–286
- Gijzen FJH, van de Vosse FN, Janssen JD (1999) Influence of the non-Newtonian properties of blood on the flow in large arteries: Unsteady flow in a 90 degree curved tube. *J Biomech* 32(7):705–713
- Gill RW (1985) Measurement of blood flow by ultrasound: accuracy and sources of error. *Ultrasound Med Biol* 11:625–641
- Hart DP (2000) Super-resolution PIV by recursive local-correlation. *J Vis* 3(2):187–194

- Jensen JA, Munk P (1998) A new method for estimation of velocity vectors. *IEEE Trans Ultrason Ferroelectr Freq Control* 45(3):837–851
- Kim HB, Hertzberg J, Lanning C, Shandas R (2004a) Noninvasive measurement of steady and pulsating velocity profiles and shear rates in arteries using echo PIV: in vitro validation studies. *Ann Biomed Eng* 32(8):1067–1076
- Kim HB, Hertzberg JR, Shandas R (2004b) Development and validation of echo PIV. *Exp Fluids* 36:455–462
- Krams R, Bambi G, Guidi F, Helderma F, van der Steen AFW, Tortoli P (2005) Effect of vessel curvature on Doppler derived velocity profiles and fluid flow. *Ultrasound Med Biol* 31(5):663–671
- Ku D, Giddens DP, Zarins CK, Glagov S (1985) Pulsatile flow and atherosclerosis in the human carotid bifurcation. *Arteriosclerosis* 5:293–302
- Liu L, Zheng H, Williams L, Zhang F, Wang R, Hertzberg J, Shandas R (2008) Development of a custom-designed echo particle image velocimetry system for multi-component hemodynamic measurements: system characterization and initial experimental results. *Phys Med Biol* 53:1397–1412
- Meinders JM, Brands PJ, Willigers JM, Kornet L, Hoeks APG (2001) Assessment of the spatial homogeneity of artery dimension parameters with high frame rate 2-d b-mode. *Ultrasound Med Biol* 27(6):785–794
- Overbeck JR, W BK, Strandness DE (1992) Vector Doppler: Accurate measurement of blood velocity in two dimensions. *Ultrasound Med Biol* 18:19–31
- Paeng D, Chiao RY, Shung KK (2004a) Echogenicity variations from porcine blood i: the “bright collapsing ring” under pulsatile flow. *Ultrasound Med Biol* 30(1):45–55
- Paeng D, Chiao RY, Shung KK (2004b) Echogenicity variations from porcine blood ii: the “bright collapsing ring” under oscillatory flow. *Ultrasound Med Biol* 30(6):815–825
- Rabben SI, Stergiopoulos N, Hellevik LR, Smiseth OA, Slordahl S, Urheim S, Angelsen B (2004) An ultrasound-based method for determining pulse wave velocity in superficial arteries. *J Biomech* 37:1615–1622
- Ramnarine KV, Nassiri DK, Hoskins PR, Lubbers J (1998) Validation of a new blood-mimicking fluid for use in Doppler flow test objects. *Ultrasound Med Biol* 24(3):451–459
- Sandrin L, Manneville S, Fink M (2001) Ultrafast two-dimensional ultrasonic speckle velocimetry: a tool in flow imaging. *Appl Phys Lett* 1155–1157
- Trahey GE, Allison JW, Von Ramm OT (1987) Angle independent ultrasonic detection of blood flow. *IEEE Trans Biomed Eng* 34(12):965–967
- Udesen J, Jensen JA (2003) Experimental investigation of transverse flow estimation using transverse oscillation. In: *Proceedings of IEEE Ultrasonics Symposium*, pp 1586–1589
- Udesen J, Jensen JA (2004) An in-vivo investigation of transverse flow estimation. *Proc SPIE* 5373:307–314
- van de Vosse FN, de Hart J, van Oijen CHGA, Bessems D, Gunther TWM, Segal A, Wolters BJBM, Stijnen JMA, Baaijens FPT (2003) Finite-element-based computational methods for cardiovascular fluid-structure interaction. *J Eng Math* 47(3-4):335–368
- van den Broek CN, Pullens RA, Frobert O, Rutten MCM, den Hartog WF, van de Vosse FN (2008) Medium with blood-analog mechanical properties for cardiovascular tissue culturing. *Biorheology* 45(6):651–661
- Westerweel J (1993) Digital particle image velocimetry—theory and application. PhD thesis, Delft University, The Netherlands
- Westerweel J, Dabiri D, Gharib M (1997) The effect of a discrete offset on the accuracy of cross-correlation analysis of digital PIV recordings. *Exp Fluids* 23:20–28
- Yuan YW, Shung KK (1989) Echogenicity of whole blood. *J Ultrasound Med* 8:425–434